OVS. In press, 2001

COMPARING LASER RAY TRACING, SPATIALLY RESOLVED REFRACTOMETER AND HARTMANN-SHACK SENSOR TO MEASURE THE OCULAR WAVE ABERRATION

Esther Moreno-Barriuso[*], PhD, **Susana Marcos**[*1], PhD, **Rafael Navarro**[*], PhD, **Stephen A. Burns**[†], PhD

[*]Instituto de Optica "Daza de Valdés", Consejo Superior de Investigaciones Científicas (C.S.I.C.), Serrano 121, 28006 Madrid, Spain

[†] Schepens Eye Research Institute, 20 Staniford St., Boston MA 02114, USA.

1. Corresponding author

Abstract

PURPOSE: To compare quantitatively three techniques to measure the optical aberrations of the human eye: Laser Ray Tracing (LRT), Hartmann-Shack wavefront sensor (HS) and Spatially Resolved Refractometer (SRR). LRT and HS are objective imaging techniques whereas the SRR is psychophysical. **METHODS:** Wave aberrations were measured in two normal subjects with all three techniques, as implemented in two different laboratories. **RESULTS:** We compared the experimental variability of the results obtained within each technique with the overall variability across the three methods. For the two subjects measured (RMS wavefront error 0.5 μm and 0.9μm respectively), we found a close agreement; the average standard deviation of the Zernike coefficients within a given method was 0.07 μm, whereas the average global standard deviation across techniques was 0.09μm, which is only slightly higher. **CONCLUSIONS:** There is a close match between the Zernike coefficients obtained by LRT, HS, and SRR. Thus, all three techniques provide similar information concerning the wave aberration, when applied to normal human eyes. However, the methods are operationally different and each presents advantages and disadvantages depending on the particular application.

Keywords: Ocular aberrations, Laser Ray Tracing, Hartmann-Shack, Spatially Resolved Refractometer, Aberrometer

In recent years, there has been a renewed effort to develop techniques for estimating the wave aberration of the human eye[1-7], partly stimulated by the interest in assessing the changes in optical quality produced by refractive surgery[8,9] and by the desire to compensate the ocular aberrations to achieve diffraction-limited optics[10-12].

Although a large number of techniques are now available, little work has been done so far to assess their equivalence[13-15] or to establish which technique is best suited for a particular situation. In the current study three different techniques, Laser Ray Tracing (LRT), the Spatially Resolved Refractometer (SRR), and the Hartmann-Shack Wavefront Sensor (H-S), have been compared in two subjects. Their principle and optical set-ups have been thoroughly described elsewhere[3,4,16]. The LRT and the H-S are objective techniques whereas the SRR is a psychophysical one. They all share a common basic principle[17]: The eye's pupil is sampled at a set (ξ_i, η_i), for i=1,…n, of locations forming a given pattern. The raw data represent the set of ray aberrations $[\Delta x'(x_i,h_i), \Delta y'(x_i,h_i)]$ corresponding to those pupil locations[1], and are proportional to the slope, or partial derivatives, of the Wave Aberration (W)[18]:

$$\Delta x' = \frac{1}{R_p}\frac{\partial W(\bar{x},\bar{h})}{\partial \bar{x}}; \qquad \Delta y' = \frac{1}{R_p}\frac{\partial W(\bar{x},\bar{h})}{\partial \bar{h}} \tag{1}$$

where $\bar{x} = x / R_p$, $\bar{h} = h / R_p$ are dimensionless canonical pupil coordinates and R_p is the pupil radius. Ray aberrations are also given in dimensionless tangent units. If they are small, the tangent is equal to the angle.

The joint representation of all the raw data $[\Delta x'(x_i,h_i), \Delta y'(x_i,h_i)]$, for i=1,…n, constitutes the spot diagram, which can be taken as a rough estimate of the shape of the retinal PSF[4]. Instead of directly integrating Eq. 1 to estimate W, it is

[1] The raw data correspond to the average slope of the wave aberration over this sample area. This value is associated to the pupil location of the center of the sample beam for further data fitting. This is a good approximation in normal eyes. See Ref. 2 (Sections 2F and ·3ª) for further details.

numerically more stable to consider an expansion of W in terms of Zernike Polynomials. Here we have considered a 7th order approximation; that is, 35 terms[19]:

$$W(\bar{x},\bar{h}) \approx \sum_{k=1}^{35} Z_k * P_k(\bar{x},\bar{h}) \qquad (2)$$

where Z_k are the coefficients of the expansion, in microns, and P_k are dimensionless Zernike polynomials.

By computing the partial derivatives of Eq. (2) and substituting them in Eq. (1), the wave aberration is estimated by a standard least squares fitting of the raw data to the partial derivatives of the Zernike polynomials for each pupil location sampled[20].

The experimental approach differs between techniques. Fig. 1a, b and c show simplified schematic diagrams of the setups. In the LRT (Fig. 1a), a set of parallel laser Gaussian pencils is sequentially delivered onto the eye through different pupil locations (ξ_i, η_i). Each ray forms a Gaussian spot on the retina (assuming that for the size of the entry beam, 2.07 mm, the effective pupil is diffraction limited) and an aerial image of the retina (which is the cross-correlation of the retinal PSF with the Gaussian spot[21]) is then relayed onto a CCD camera. The image is recorded and its centroid is subsequently computed as a maximum-likelihood estimate of its position (X'(ξ_i, η_i), Y'(ξ_i, η_i)). The joint plot of all the centroids constitutes the spot diagram. In the presence of aberrations, the spots (located in (X',Y')) are displaced from their reference positions(X' = X'$_0$; Y' = Y'$_0$), and the geometrical aberration is defined by the magnitude of these displacements (given here in dimensionless tangent units):

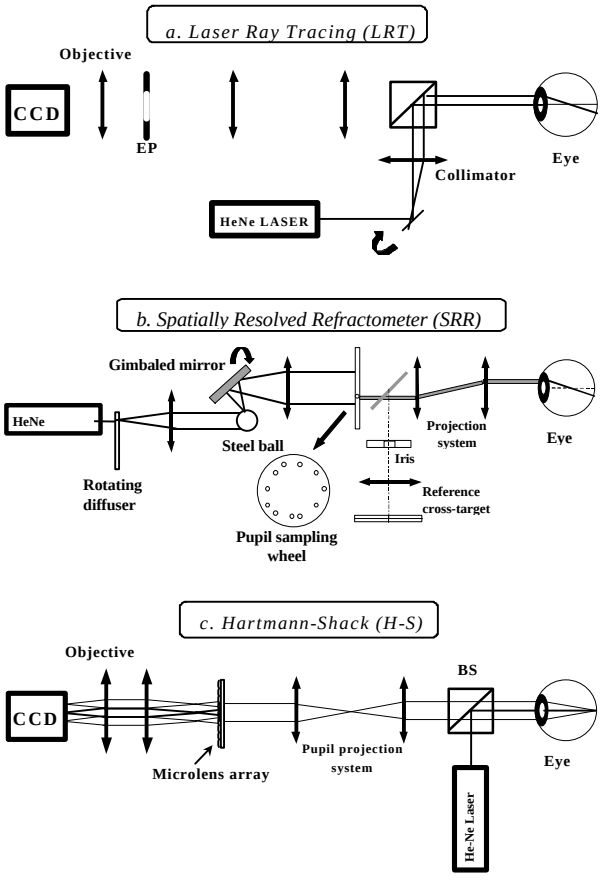

Figure 1 – Schematic diagrams of the basic setup for the three techniques: a) Laser Ray Tracing, b) Spatially Resolved Refractometer, c) Hartmann-Shack wavefront sensor (See text for details)

$$\Delta x'(x_i,h_i) = \left[X'(x_i,h_i) - X'_0(x_i,h_i)\right]$$
$$\Delta y'(x_i,h_i) = \left[Y'(x_i,h_i) - Y'_0(x_i,h_i)\right] \qquad (3)$$

We use a unique reference in LRT ($X'_0(x_i,h_i) = X'_0, \quad Y'_0(x_i,h_i) = Y'_0, \ \forall i$), which is the location of the spot for the chief ray. In LRT the first-pass is the measurement pass, while in the second-pass all rays are affected equally by the overall aberrations (assuming isoplanatism).

The SRR (see Fig. 1b), is a psychophysical technique. As in LRT, the pupil is sampled by sequentially projecting diffraction-limited apertures (drilled in a spinning wheel) at different locations (ξ_i, η_i) on the eye's pupil. A focusing block (not shown in Fig 1b) allows for defocus compensation. Due to the aberrations, the subject will perceive the spots in different retinal locations. For each entry pupil, the task consists of tilting the incoming beam a given angle along both axes (α_X (ξ_i, η_i), α_Y (ξ_i, η_i)) by means of a joystick until he/she perceives the spot aligned to a reference cross, viewed through the center of the pupil (see reference channel in Fig. 1b). The tilt equals the wavefront slope but with opposite sign so that the ray aberration is cancelled out. The ray aberration $\left[\Delta x'(x_i,h_i), \Delta y'(x_i,h_i)\right]$ is computed from Eq. (3) using (X'(ξ_i, η_i), Y'(ξ_i, η_i)) = (-α_X (ξ_i, η_i), -α_Y (ξ_i, η_i)), and considering the center of the pupil as the aberration-free reference.

In the H-S wavefront sensor (Fig. 1c), a monolithic microlens array, located in a plane conjugate to the exit pupil, samples the wavefront in parallel. Each lenslet selects a portion of the wavefront of the size of the lenslet and forms a spot of light at its focal plane. A single snapshot provides a grid of image spots, which is imaged onto a CCD camera. Each spot is the cross-correlation between the eye's PSF (first-pass)

Table 1 - Specifications for Laser Ray Tracing, Spatially Resolved Refractometer and Hartmann-Shack Wavefront Sensor implemented for this study

	LRT	SRR	HS
Objective / psychophysical	Objective	Psychophysical	Objective
Parallel/ sequential	Sequential	Sequential	Parallel
Number of samples taken:	37	37	91[1]
Sample diameter (mm)	~ 0.6	1	0.5[1]
Sampling step (mm)	1	1	0.6[1]
Sampling pattern (shape):	Rectangular	Rectangular	Hexagonal
Effective pupil sampled[2](mm):	6.6	7.2	6.6
Measurement in first/second pass:	First	First	Second
Entry pupil size (mm)	~ 0.6	1	~ 0.6
Exit pupil size (mm)	3[3]	N/A	0.5[4]
Wavelength (nm)	543	543	543
# of runs averaged for each subject	4	4	4
Mydriasis:	1 drop cyclopentolate 1%	No Mydriasis required 1 drop cyclopentolate1% in these measurements	1 drop cyclopentolate1%
Light level required	~ 10μW	~0.1μW (Photopic)[5]	~ 30μW
Duration of the measurement	~5s	~3 or 4 min.	~2s
Area available for each aerial image (pixels)	64x64	N/A	15x15
Compensation of defocus (although measurements here were uncorrected)	Trial lenses	Focusing block (mirrors)	Trial lenses
Zernike terms fitted	35	35	35

[1] Specifications of the microlens array: focal length f' = 50mm; clear aperture = 500μm; lenslet interdistance = 600 μm; hexagonal arrangement.
[2] The effective pupil diameter is the distance from the pupil center required for all the light from each aperture to enter (or exit) the eye. For each technique, the wave aberration was computed for the corresponding effective pupil size, and then the Zernike coefficients are recalculated for the smallest pupil (6.6 mm) to allow direct comparison.
[3] Artificial pupil located in a plane conjugate to the eye's pupil
[4] Equal to the microlens diameter
[5] Retinal illuminance is about 10 td, when considering both the measurement beam and the extended background field.

and that of a single microlens (second, measurement pass). For an aberration-free eye, the emerging wavefront is flat and thus, the grid of image spots has a spatial distribution ($X_0'(\xi_i, \eta_i)$, $Y_0'(\xi_i, \eta_i)$) identical to that of the microlenses themselves. In the presence of aberrations, the image spots ($X'(\xi_i, \eta_i)$, $Y'(\xi_i, \eta_i)$) are shifted from their reference position. This shift is proportional to the average slope of the wavefront across the microlens pupil (see Eq. 1). By applying Eq. 3, subtracting the test from the reference coordinates of the centroids, we obtain the geometrical aberrations $\left[\Delta x(x_i, h_i), \Delta y(x_i, h_i)\right]$ and the spot diagram.

Table 1 summarizes the characteristic features of each of the three techniques, both the ones inherent to the method itself, and the ones due to the particular setup employed for this experiment (but that could be modified in alternative implementations). For this comparative study, two different laboratories were involved: we used the SRR built at the Schepens Eye Research Institute (Boston, USA)[2], while the H-S sensor and the LRT technique were implemented at the Institute of Optics (Madrid, Spain)[14]. The experimental conditions were kept as similar as possible taking into account the inherent differences among methods.

Two subjects, one male aged 41 (RN) and one female aged 25 (EM), participated in the study, both using their right eye. In all three types of measurements defocus was left uncorrected (-1.5D for RN and –0.5D for EM). Measurements were carried out over a 2-year period. For each instrument, sessions consisted of 4 runs of measurements, from which the set of average Zernike coefficients (for comparison between techniques) and the corresponding standard deviation (for variability estimation within each technique) were computed. The resulting Zernike coefficients are shown in Fig. 2 for subject RN (2a) and for subject EM (2b). Solid triangles stand for SRR, open circles for LRT, and solid squares for H-S. Each symbol is the average value over 4 runs. The error bars (representing the standard deviation of each technique) have not been depicted for the sake of clarity, as they are, in all cases, of the same size as the symbol or smaller**.** The ordering for the Zernike polynomials corresponds to that recommended by the OSA Standardization Committee[22]. We have assessed the variability within a technique by computing the standard deviation of each Zernike coefficient across runs in a session, and then taking the average across coefficients. The standard deviation within each technique has been compared with the average standard deviation across techniques. For this purpose we have averaged the set of Zernike Coefficients obtained with LRT, SRR and H-S, computed the standard deviation of each

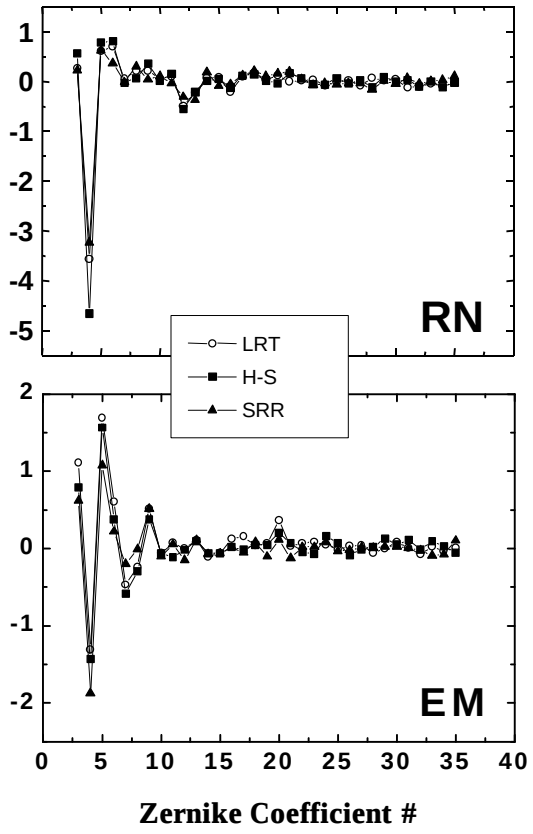

Figure 2 – Zernike Coefficients for the three techniques, for subjects RN (upper) and EM (lower). Triangles stand for SRR, open circles for LRT, and solid squares for HS. Each symbol is the average across 4 runs. Errors bars (not shown) are the same size or smaller than the symbols in all case.

individual coefficient and then averaged these values across the coefficients. Averaging has been done either for coefficients 3-35 (orders 2-7) or for coefficients 3-14 (orders 2-4), to analyze possible changes across orders.

There is a close match among the three techniques: For RN (RMS wavefront error 0.5 μm) the average standard deviation across data (Zernike Coefficients) from an individual technique is 0.071 μm (0.066 μm for H-S, 0.063 for LRT and 0.084 for SRR), while the average standard deviation across the three techniques is 0.09 μm. For subject EM (RMS wavefront error 0.9 μm), the average standard deviation of data from individual techniques is 0.065 μm, whereas the average standard deviation across the three techniques is again 0.09 μm. The main contribution to the slight mismatch across techniques is due to the low-order aberrations, which present the largest aberration values. Considering only orders 2 to 4 (coefficients 3 to 14), the average standard deviation across techniques is 0.16 μm, and the standard deviation within a technique is 0.09 μm, for RN; the standard deviations are 0.14 μm and 0.08 μm, respectively, for EM. The main contribution to the larger inter-technique standard deviation is due to the defocus term, which is the one most likely to change across sessions due to the variation of the accommodative state reached by the subject after instillation of the mydriatic agent.

Fig. 3 shows contour plots of the wave aberration for RN for each of the 3 methods. Tilt terms (Z1, Z2) and defocus (Z_4) have been cancelled in these plots to enhance the high-order features of the wave aberration, showing also the equivalence of the three methods for the measurement of optical aberrations in normal subjects. Nevertheless, given their different nature, each one can present advantages or limitations, depending on the specific application.

Below we present a summary of the results of this study, together with the main differences among the three techniques. We emphasize both issues that are inherent to the nature of each method and issues related to our particular implementation:

1.- For the two normal subjects presented here the three methods are equivalent. However, some differences may arise when measuring clinical eyes. On the one hand, for eyes with considerable amounts of wave aberrations LRT and SSR may be more robust than HS due to their sequential nature. That is, since they are sequential, they do not suffer from indexing problems[8], which may appear in H-S if the grid of image spots is too distorted. On the other hand, the computation of the centroid may be affected by speckle noise and the limited number of pixels/spot in the H-S[14]; when the spots are too distorted (for highly aberrated eyes) and the boundary between adjacent spots is not clear, the centroid computation become difficult, even for a diffraction-limited first pass[14]. This may limit its range of application, especially in some clinically interesting cases. Alternative light sources (such as superluminescent diodes) have been suggested, to overcome the speckle noise problem in the H-S. This limitation is reduced in LRT, in which the entire CCD is used for each spot. In SRR the only limitation is the ability of the subject to align the image spot and the dynamic range of the gimbaled mirror.

2.- Measurements with the LRT and the H-S rely on a good retinal reflection, which might be a problem in abnormal retinas[23]. This is not a hindrance for the SRR; however, the SRR requires proper light capture by the photoreceptors and good fixation. These requirements could be a disadvantage for some classes of patients.

3.- The sequential nature of LRT and SRR limits their application for real-time dynamic measurements. H-S is the fastest technique (1 or 2 seconds), and speckle removal techniques can be applied to take faster real-time dynamic recordings[24]. In the present configuration, the duration of each exposure in LRT can be reduced to ~50 ms without being limited by speckle noise[14], the main constraint in duration of a measurement being the speed of the imaging board.

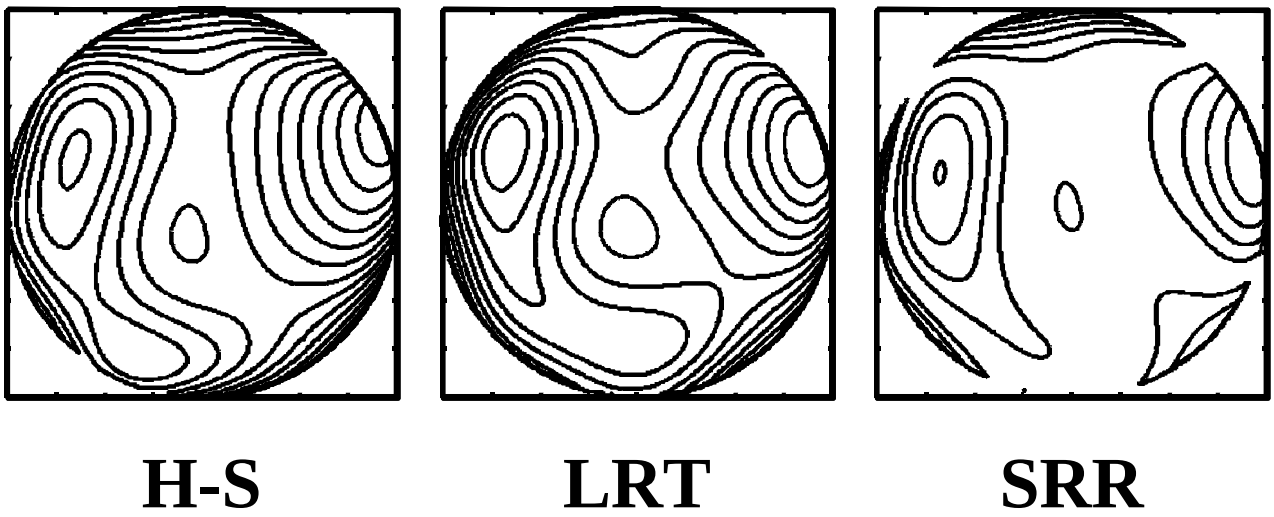

Figure 3 - Contour plots of the wave aberration for the right eye of subject RN, for H-S (left), LRT (center) and SRR (right) measurements. Left represents temporal side, and right represents nasal side. Pupil coordinates range from –3.25 mm to 3.25 mm. Step between adjacent contour lines is 0.5 μm.

This implementation requires 5 seconds for 37 rays. An SRR run takes 3 to 4 minutes due to its psychophysical nature. Although eye movements, fluctuations of accommodation, etc., may be thought to be more important problems for the slowest techniques, we did not find a trend for increased variability with a particular technique: for RN, SRR was the noisiest (0.083 μm), for EM it was the H-S (0.09 μm).

The following two aspects are related to the particular implementation of the technique employed in the study, and thus could be overcome in future version of the system.

1.- All three systems operate with visible light (although some versions of H-S with IR light have already been used by other groups[24]), and as a result, pupil dilation is required for H-S and LRT in order to avoid reflex pupil constriction. The SRR uses light levels sufficiently low to operate with a natural pupil for most subjects (although for this work, a midriatic was used for comparison with the other methods. In this sense, it can therefore be more comfortable for the subject.

2.- H-S uses a fixed monolithic microlens array, whose sampling configuration cannot be modified unless different microlens arrays are used- In the SRR version used in this work, the sampling pattern provided by the wheel was also fixed, although programmable masks are possible[25]. In LRT, the laser scanner can be flexibly programmed to change the sampling pattern's shape (rectangular, hexagonal, polar). This allows the sampling pattern to be adapted to individual cases (i.e. normal versus refractive surgery patients), or even the use of a non-homogeneous sampling pattern[26]. Even if the sampling step size can be changed easily, the sample's size (given by the beam waist size) remains unchanged, which affects the "filling factor" (fraction of the pupil covered by the sampling pattern).

In summary, we have demonstrated experimentally the equivalence of three different techniques for measuring ocular aberrations in normal human eyes: the Laser Ray Tracing, the Spatially Resolved Refractometer and the Hartmann-Shack wavefront sensor. The particular features of each technique (see table) make one or the other more convenient depending on the specific problem or application.

ACKNOWLEDGEMENTS:

We thank Mike Hutley for providing us with the microlens array employed in the experiments. This research has been supported by the Comisión Interministerial de Ciencia y Tecnología of Spain, grant TIC98-0925-C02-01, by the grant EYO4395 and by the Human Frontier Science Program LT-542/97.

REFERENCES

1. - Walsh G, Charman WN, and Howland HC. Objective technique for the determination of monochromatic aberrations of the human eye. J. Opt. Soc. Am. A 1984;1:987-992.

2. - He JC, Marcos S, Webb RH, and Burns SA. Measurement of the wave-front aberration of the eye by a fast psychophysical procedure. J. Opt. Soc. Am. A 1998;15:2449-2456.

3. - Liang J, Grimm B, Goelz S, and Bille J. Objective measurement of wave aberrations of the human eye with the use of a Hartmann-Shack wave-front sensor. J. Opt. Soc. Am. A 1994;11:1949-1957.

4. - Navarro R and Losada MA. Aberrations and relative efficiency of light pencils in the living human eye. Optom. Vis. Sci. 1997;74:540-547.

5. - Liang J and Williams DR. Aberrations and retinal image quality of the normal human eye. J. Opt. Soc. Am. A 1997;14:2873-2883.

6. - Iglesias I, Berrio E, and Artal P. Estimate ocular wave aberration from pairs of dou retinal images. J- Opt. Soc. Am. A 1998;1 2476.

7. - Mierdel P, Krinke HE, Wiegand W, Kaemmerer M, and Seiler T. Measuring device for determining monochromatic aberration of the human eye. Ophthalmologe 1997;94:441-445.

8. - Thibos L and Hong X. Clinical applications of the Shack-Hartmann aberrometer. Optom. Vis. Sci. 1999;76:817-825.

9. - Oshika T, Klyce SD, Applegate RA, Howland HC, and El Danasoury MA. Comparison of corneal wavefront aberrations after photorefractive keratectomy and laser in situ keratomileusis. Am. J. Ophthalmol. 1999;127:1-7.

10. - Liang J, Williams DR, and Miller D. Supernormal vision and high resolution retinal imaging through adptive optics. J. Opt. Soc. Am. A 1997;14:2884-2892.

11. - Zhu L, Sun P, Bartsch D, Freeman WR, and Fainman Y. Adaptive control of a micromachined continous-membrane deformable mirror for aberration compensation. Appl. Opt. 1999;38:168-176.

12. - Navarro R, Moreno-Barriuso E, Bará S, and Mancebo T. Phase-plates for wave-aberration compensation in the human eye. Opt. Lett. 2000;25:**.

13. - Salmon T, Thibos L, and Bradley A. Comparison of the eye´s wave-front aberration measured psychophysically and with the Shack-Hartmann wave-front sensor. J. Opt. Soc. Am. A 1998;15:2457-2465.

14. - Navarro R and Moreno-Barriuso E. Laser Ray-Tracing versus Hartmann-Shack Sensor for Measuring Aberrations in the Eye. In: Technical Digest Opt. Soc. Am. Annual Meeting, 71, Baltimore (USA), 1998:71.

15. - Thibos L and Hong X. Comparison of monochromatic aberrations of the human eye measured with the Howland crossed-cylinder aberroscope and the Shack-Hartmann aberrometer. In: Technical Digest Optical Society of America Annual Meeting, 55, Santa Clara, California (USA), 1999:55.

16. - Webb RH, Penney CM, and Thompson KP. Measurement of ocular wavefrontdistortion with a spatially resolved refractometer. Appl. Opt. 1992;31:3678-3686.

17. - Smirnov MS. Measurement of the wave aberration of the human eye. 1961;776-795.

18. - Born M and Wolf E. Principles of Optics. 6th, Oxford, U.K.: Pergamon Press, 1993.

19. - Malacara D. Optical Shop Testing. 2nd ed., New York: John Wiley & Sons, Inc., 1992.

20. - Southwell WH. Wave-front estimation from wave-front slope measurements. J. Opt. Soc. Am. A. 1980;70:998-1006.

21. - Navarro R and Losada MA. Phase transfer and point-spread function of the human eye determined by a new asymmetric double-pass method. J.Opt.Soc.Am. A 1995;12:2385-2392.

22. - Thibos LN, Applegate RA, Schwiegerling JT, Webb RH, and Members VST. Standards for reporting the optical aberrations of eyes. Vision Science and its Applications TOPS Volume 2000;35:

23. - Elsner AE, Burns SA, Weiter JJ, and Delori FC. Infrared imaging of sub-retinal structures in the human ocular fundus. Vis. Res. 1996;36:191-205.

24. - Hofer HJ, Porter J, and Williams DR. Dynamic Measurement of the Wave Aberration of the Human Eye. Invest. Ophth. & Vis. Sci. 1998;39 (Suppl.):

25. - Webb RH, Burns SA, and Penney M. Coaxial Spatially Resolved Refractometer. United States Patent 6,000,800 1999;

26. - Rios S, Acosta E, and Bara S. Hartmann sensing with Albrecht grids. Opt. Comm. 1997; 133:443-453.